Am J Physiol Heart Circ Physiol 317: H279–H289, 2019.
First published May 31, 2019; doi:10.1152/ajpheart.00510.2018.

RESEARCH ARTICLE | *Adaptive Immunity in Cardiovascular Disease*

Elevated bone marrow sympathetic drive precedes systemic inflammation in angiotensin II hypertension

Niousha Ahmari,[1,2] Monica M. Santisteban,[2] Douglas R. Miller,[3] Natalie M. Geis,[1] Riley Larkin,[1] Ty Redler,[1] Heather Denson,[1] Habibeh Khoshbouei,[3] David M. Baekey,[1] Mohan K. Raizada,[2] and Jasenka Zubcevic[1]

[1]*Department of Physiological Sciences, College of Veterinary Medicine, University of Florida, Gainesville, Florida;*
[2]*Department of Physiology and Functional Genomics, College of Medicine, University of Florida, Gainesville, Florida; and*
[3]*Department of Neuroscience, College of Medicine, University of Florida, Gainesville, Florida*

Submitted 27 July 2018; accepted in final form 25 May 2019

Ahmari N, Santisteban MM, Miller DR, Geis NM, Larkin R, Redler T, Denson H, Khoshbouei H, Baekey DM, Raizada MK, Zubcevic J. Elevated bone marrow sympathetic drive precedes systemic inflammation in angiotensin II hypertension. *Am J Physiol Heart Circ Physiol* 317: H279–H289, 2019. First published May 31, 2019; doi:10.1152/ajpheart.00510.2018.—Increased sympathetic nervous system activity is a hallmark of hypertension (HTN), and it is implicated in altered immune system responses in its pathophysiology. However, the precise mechanisms of neural-immune interaction in HTN remain elusive. We have previously shown an association between elevated sympathetic drive to the bone marrow (BM) and activated BM immune cells in rodent models of HTN. Moreover, microglial-dependent neuroinflammation is also seen in rodent models of HTN. However, the cause-effect relationship between central and systemic inflammatory responses and the sympathetic drive remains unknown. These observations led us to hypothesize that increase in the femoral BM sympathetic nerve activity (fSNA) initiates a cascade of events leading to increase in blood pressure (BP). Here, we investigated the temporal relationship between the BM sympathetic drive, activation of the central and peripheral immune system, and increase in BP in the events leading to established HTN. The present study demonstrates that central infusion of angiotensin II (ANG II) induces early microglial activation in the paraventricular nucleus of hypothalamus, which preceded increase in the fSNA. In turn, activation of fSNA correlated with the timing of increased production and release of $CD4^+$.$IL17^+$ T cells and other proinflammatory cells into circulation and elevation in BP, whereas infiltration of $CD4^+$ cells to the paraventricular nucleus marked establishment of ANG II HTN. This study identifies cellular and molecular mechanisms involved in neural-immune interactions in early and established stages of rodent ANG II HTN.

NEW & NOTEWORTHY Early microglia activation in paraventricular nucleus precedes sympathetic activation of the bone marrow. This leads to increased bone marrow immune cells and their release into circulation and an increase in blood pressure. Infiltration of CD4+ T cells into paraventricular nucleus paraventricular nucleus marks late hypertension.

angiotensin II; hypertension; inflammation; neuroinflammation; SNS

INTRODUCTION

Evidence supports a major role for activated immune system (IS) in pathophysiology of hypertension (HTN) and cardiovascular disease (19). In experimental rodent models, the IS relies on the presence of circulating T cells, among other inflammatory markers, for establishment of ANG II-dependent HTN (15). Our recent work demonstrated that a proinflammatory bone marrow (BM) is a significant source of inflammatory cells (ICs) in HTN, including T cells and monocyte/macrophages (21, 35). These can infiltrate the paraventricular nucleus (PVN), and their infiltration has been linked with neuroinflammatory responses and dysfunction of the autonomic nervous system (ANS) (21).

An imbalance in IS-ANS communication has been proposed in cardiovascular disease, as dysregulation of ANS is associated with elevated production and release of BM-derived ICs into circulation in HTN and heart disease (10, 35). In support of this, genetic blockade of BM β-adrenergic receptors causes a significant drop in blood pressure (BP) that is associated with a reduction in the levels of circulating ICs, including the $CD4^+$ T cells and monocyte/macrophages (6). Considering the dynamic interplay between the IS and ANS (4), and the dysfunction in both systems in established HTN, an investigation of the temporal relationship between activation of the IS, dysfunction of ANS, and BP increase is warranted to propose possible causative mechanisms in early and late stages of ANG II-dependent HTN.

The current study demonstrates that the early stage of rodent ANG II HTN displays microglial-dependent neuroinflammation that precedes an elevation in BM sympathetic drive. The latter in turn initiates systemic inflammatory responses that originate in the BM in concurrence with elevation in BP. Establishment of ANG II HTN coincides with infiltration of ICs into the PVN, which may further exacerbate neuroinflammation and ANS dysfunction.

METHODS

Animal models. All experimental procedures were approved by the University of Florida Institute of Animal Care and Use Committee and complied with the standards stated in the National Institutes of Health Guide for the Care and Use of Laboratory Animals. Sprague-Dawley rats (male, 4–14 wk old; weight, 50–350 g) were purchased from Charles River and housed separately in a temperature-controlled

Address for reprint requests and other correspondence: J. Zubcevic, Dept. of Physiological Sciences, College of Veterinary Medicine, University of Florida P.O. Box 100274 Gainesville, FL 326100274 (e-mail: jasenkaz@ufl.edu).

room (22–23°C) with a 12-h:12-h light-dark cycle, in specific pathogen-free cages, and had access to standard rat chow and water ad libitum. All animals were under care of the University of Florida Animal Care Services throughout the experiments.

Chronic ANG II infusion and blood pressure measurements in rats in vivo. We used a low dose of ANG II to slowly induce ANG II HTN to investigate a temporal relationship between activation of the BM sympathetic drive, IS responses, and BP. Radio-transmitter implantation (DSI) was performed as previously described (21, 35). Briefly, adult (12–14 wk old, $n = 48$) male Sprague-Dawley rats were anesthetized with 2% isoflurane. Rat telemeters (PA-C40; Data Sciences International) were implanted into the abdominal aorta for chronic measurements of BP in unrestrained conscious rats. All animals received buprenorphine (0.1 mg/kg) for pain management and were allowed to recover for 1 wk before baseline BP measurements. Baseline systolic BP (SBP) and mean BP (MBP) were recorded for 48 h before implantation of pumps for chronic ANG II or artificial cerebrospinal fluid (ACSF) infusion. Animals were randomly assigned to either the control (ACSF) or ANG II experimental group ($n = 24$ per group). Chronic ANG II infusion (100 ng/h icv) was performed using mini-osmotic pumps (ALZET 2004) implanted subcutaneously, with intracerebroventricular catheters inserted through the skull and secured in place using dental cement. Control animals received ACSF for 3, 7, 14, and 21 days of continuous intracerebroventricular infusion ($n = 6$ per group), and the experimental groups received ANG II in ACSF for 3, 7, 14, and 21 days of continuous intracerebroventricular infusion ($n = 24$). SBP and MBP were recorded for 24 h continuously at designated days after the start of ANG II infusion. Data are presented as means ± SE.

Decorticated artificially perfused rat preparation and femoral bone marrow sympathetic nerve recordings in situ. We performed direct electrophysiological recordings of femoral sympathetic nerve activity (fSNA) innervating the BM via the femoral nutrient foramen as previously described (36). Juvenile (male, 4–6 wk old, 50–60 g, $n = 24$) Sprague-Dawley rats were purchased from Charles River and used for the in situ rat preparation. After their arrival, rats were allowed to recover for 3 days before chronic ANG II or ACSF infusion. Chronic ANG II infusion (100 ng/h icv, $n = 6$ per time point) was performed as described above. Control animals received ACSF for 3 and 7 days of continuous intracerebroventricular infusion ($n = 6$ per time point), whereas the experimental groups received ANG II in ACSF for 3 and 7 days of continuous intracerebroventricular infusion ($n = 6$ per time point). Rats were randomly assigned to the experimental groups. The time points of infusion were chosen to establish the time course of fSNA changes before increase in SBP/MBP, as per the in vivo SBP measurements in conscious rats. At *days 3* and *7* of ANG II infusion, rats were anesthetized, exsanguinated, decorticated, and immediately submerged into ice-chilled ACSF, comprised of (in mM) 125 NaCl, 24 $NaHCO_3$, 3KCl, 2.5 $CaCl_2$, 1.25 $MgSO_4$ and 1.25 KH_2PO_4, 10 dextrose (pH 7.3) (Sigma-Aldrich and Fisher). The skin, viscera, and lungs were removed, and the left phrenic nerve was isolated. The preparation was then transferred to an acrylic perfusion chamber, cannulated through the left ventricle with a double lumen catheter (Braintree Scientific). The preparation was immediately perfused with warmed Ringer's solutions (32–33°C) containing Ficoll PM70 (1.25%, Sigma-Aldrich) bubbled with 95% O_2-5% CO_2 and pumped through two in-line bubble traps and a filter (polypropylene mesh; pore size, 40 μm; Millipore) using a peristaltic pump. Neuromuscular paralysis was produced by addition of vecuronium bromide (2–4 μg/ml, Bedford) directly to the perfusate. Perfusion pressure was measured via one lumen of the double-lumen catheter using a pressure transducer connected to an amplifier. Simultaneous recordings of the phrenic nerve activity (PNA) and the fSNA were obtained using glass suction electrodes (tip diameter, 0.2–0.3 mm), amplified (20–50 K) and filtered (3–30 K), sampled at 5 kHz (CED, Cambridge), and monitored using Spike2 (CED). The perfusate flow (19–24 ml/min) was adjusted until an augmenting (i.e., eupneic) pattern of PNA was achieved. Vasopressin (1.25–4 nM final concentration, Sigma-Aldrich) was added to the perfusate to increase vascular resistance and maintain perfusion pressure. fSNA recording and comparison between control and ANG II-infused rats were performed. For data analysis and comparison, phrenic-triggered averaging of integrated fSNA was performed as previously described across 100 phrenic cycles (time constant = 100 ms) (35). This allowed for the classification of averaged fSNA into the phases related to the respiratory cycle: inspiration (I), postinspiration (P-I), midexpiration (M-E), and late expiration (L-E). To account for variations in cycle length between preparations, I phase was determined as time between the beginning of the PNA burst to end inspiration, and individual P-I and M-E were of a fixed duration (0.4 ms), whereas the L-E phase was estimated as the remainder of the phrenic cycle. Thus, the peak levels of fSNA during each respiratory phase could be compared across preparations.

Surgical denervation of femoral bone marrow in rat ANG II model. To confirm the role of central ANG II-dependent increase in fSNA on the BM inflammatory mediators in the rat, surgical dennervation of the femoral BM sympathetic nerve (BM SNAX) was performed unilaterally in 6 male adult (12–14 wk old, $n = 6$) Sprague-Dawley rats at the same time of ANG II intracerebroventricular infusion. For BM SNAX, rats were placed under 2% isofluane anesthesia and the left hindlimb was shaved between the abdomen and the paw and prepared for sterile surgery. The skin was excised with a scalpel to expose the superficial femoral blood vessels. With the use of blunt forceps, the nutrient foramen artery branch of the femoral artery was exposed and separated from the adjacent nerve. The nerve was then carefully dissected, leaving the nutrient foramen artery intact. The skin was closed using sterile, steel wound-closing clips. Sham surgery was performed in the opposite (right) hindlimb, in which the nutrient foramen artery was similarly exposed and separated from the adjacent nerve, but no dissection of the nerve was performed. At the same time of BM SNAX, all rats were implanted subcutaneously with ALZET pumps attached to intracerebroventricular catheters to chronically deliver ANG II (100 ng/h) for 7 days, as described above. At end point, rats were euthanized, both left and right femurs were collected, and the BM cells were separated from the BM supernatant to perform fluorescence-activated cell sorting and norepinephrine (NE) ELISA assay, respectively.

Fluorescence-activated cell sorting in rat ANG II model. Rats from the telemetry experiment described above were euthanized by isoflurane overdose, followed by immediate removal of blood, brain, and hind limbs. Rat femurs were isolated and collected in ice-cold, phosphate-buffered saline (PBS) supplemented with 1% fetal bovine serum (FBS). After each femur of all connective tissue was cleaned, the epiphyses of each bone were removed and a sterile, 21-gauge needle containing PBS with 1% FBS was used to flush marrow from each femur. BM samples were gently homogenized by pipetting and were then filtered through a 70-micron cell strainer (Corning, cat. no. 352350) to remove debris and obtain a uniform, single-cell suspension. Blood was collected in K2-EDTA-treated tubes (BDbiosciences, cat. no. 366643), and circulating mononuclear cells (MNCs) were isolated from blood using Ficoll Paque Plus (GE Healthcare) according to established protocols (5). Briefly, blood was diluted in PBS, gently layered on top of Ficoll medium, and spun at 450 *g* for 45 min at room temperature. The resulting MNC layer was collected and washed twice with ice-cold PBS + 1% FBS and filtered to obtain a uniform, single-cell suspension. After isolation, BM and MNC suspensions were aliquoted at a concentration of 0.5–1 × 10^6 cells/100 μl in PBS + 2% FBS + 1 mM EDTA mixture media, as previously described (21, 35). Prior to labeling, antibodies were titrated to determine appropriate concentration, and isotype controls were used to validate antibody specificity. Antibody labeling on live cells was performed at 4°C for 30 min. After surface staining, appropriate samples of cells were washed twice with PBS, fixed with 2% fresh paraformaldehyde, and permeabilized using Permeabilization buffer (BioLegend) for subsequent intracellular staining of IL17. Cells were

again washed and fixed following intracellular labeling. All staining was performed according to the manufacturer's protocols (see Table 1 for full antibody info). Negative and isotype controls were prepared alongside samples to enable correct compensation and confirm antibody specificity. All samples were read using an LSR-II (BD Biosystems) at the University of Florida Interdisciplinary Center for Biotechnology, and the data were analyzed with FACSDiva software, version 6.1.2.

Immunohistochemistry in the paraventricular nucleus of ANG II-infused rats. Whole brains were collected and postfixed for 48 h in a 50-ml conical tube containing 2% paraformaldehyde in PBS solution. For cryoprotection, brains were placed in 50 ml of 30% sucrose for 3–4 days (or until the samples sunk). Following cryoprotection, brains were flash-frozen in O.C.T. Compound (Tissue-Tek) and stored at −80°C until sectioning. The samples were sectioned using a cryostat at 30-μm thickness in the coronal plane, and three brain sections (from Bregma, −1.7 to −1.8 mm) per animal were mounted onto glass slides and stored at −20°C. Before immunolabeling, all samples were washed with PBS, permeabilized with 0.05% Triton X-100 for 30 min, and incubated in PBS + 10% FBS for 1 h at room temperature to saturate nonspecific binding sites. The primary antibodies used (Table 1) were rabbit polyclonal anti-Iba1 (1:1,000; Wako) to label microglial cells and infiltrating macrophages, mouse anti-NeuN (1:1,000; Millipore) to label neurons, and mouse anti-Rat CD4 (1:500; eBioscience), which is a marker present on peripheral T cells (21). Primary antibodies were incubated overnight at 4°C. Samples were then washed three times with PBS and incubated in appropriate secondary antibody (1:1,000) for 1 h (see Table 1 for full antibody list and information). Samples were finally washed five times with PBS and Fluoromount-G mounting medium with DAPI (ThermoFisher). Additional brain tissue was incubated with secondary antibodies only and used as a negative control to validate antibody specificity. Spleen and colon were used as positive controls for confirmation of CD4 antibody.

Immunolabeled slides were visualized with a Nikon A1 laser-scanning confocal microscope using either oil-immersion objectives (from ×20–90, Nikon Instruments, Meleville, NY). Excitation was achieved with 405 nm (Coherent, Santa Clara, CA), 480 nm (Melles Griot, Carlsbad, CA) and 561 nm (Coherent) laser lines in a nonoverlapping series for DAPI, Iba1, and CD4 visualization, respectively. Emission was detected at 450 nm, 525 nm, and 538 nm for DAPI, Iba1/NEUN, and CD4, respectively. All samples were imaged under identical laser power, gain, and pixel dell and treated identically for analysis. Image analysis, including cell counting and processing for representative display, was carried out in Nikon Elements (Nikon Instruments). All images were automatically denoised using Nikon Elements before analysis.

For quantification of $CD4^+$ cells, overlapping ×20 and ×40 images were taken to capture both sides of the PVN as demarcated by Paxinos and Watson Rat Brain Atlas and its location proximal to the third ventricle. CD4-positive cell counts were manually performed in the entire area of the PVN for each brain section and reported as the average of the number of total $CD4^+$ cells for each PVN slice. These were then averaged within each animal and within experimental groups and presented as means ± SE. T cells were morphologically identified as round, nucleated $CD4^+$ cells matching the morphological characteristics and size described in the literature (7, 20, 23, 33).

Image acquisition and antibody use were optimized for assessment of microglial morphology. Confocal images were collected in Z-stacks, with 2.175-μm z-step moving 16 microns above and below user-defined central plane. A single high-quality image of the entire PVN was created using Nikon Elements with 5 or 10% overlap of consecutive regions. To determine changes in microglial number, $Iba1^+$ cells were manually counted in the PVN of each brain section by two blinded individuals and data were then averaged between counts. Microglial counts within the ependymal third-ventricle border were excluded from the total counts. To automatically identify $Iba1^+$ cells, maximum intensity projections of each image were thresholded to create a binary mask, and a second binary mask was created to mark the area of the PVN. The intersection of both binary masks was used to quantify changes in microglial morphology. In addition to total cell counts, circularity was chosen as a measure of microglial cell activation and was defined in the following manner: the area and perimeter of each cell was determined from the intersected binary mask, and circularity index was automatically calculated as $4\pi(\text{area})/(\text{perimeter})^2$ (Nikon Elements).

RNA isolation and RT-PCR in rat bone marrow. RNA was isolated from BM MNCs using RNeasy Plus Mini kit (Qiagen) using TRIzol Reagent (Ambion) according to the manufacturers' protocols. Purity of RNA was evaluated spectrophotometrically by a 260-to-280 ratio. Reverse transcription was accomplished using High-Capacity Reverse Transcription kit (Applied Biosystems) and 500 ng RNA from the previous step. RT-PCR was performed using Taqman universal PCR master mix and Taqman gene expression assay primers (Applied Biosystems) listed in Table 2. Real-time PCR was run using ABI Prism 7600 sequence detection system. All cDNA samples were assayed in duplicate. Data were normalized to GAPDH and presented as means ± SE.

Norepinephrine ELISA in femoral bone marrow of rats. SHAM and BM SNAX femurs were collected, trimmed at the distal epiphysis end, and placed in a 15-ml conical tube, with the trimmed epiphysis facing the bottom and immersed in 200 μl of NE ELISA buffer. The bones were then centrifuged at 4,000 revolutions/min for 30 min at 4°C to extract the BM. The pelleted BM was briefly vortexed and centrifuged at 1,200 revolutions/min for 10 min at 4°C. After this, the BM supernatant was collected and stored at −80°C until use. The NE levels were measured using a commercially available kit (Labor Diagnostika Nord, Germany; Rocky Mountain Diagnostics; BA

Table 1. *Antibodies used for flow cytometry and brain immunohistochemistry analysis in rat*

	Antibody	Application	Vendor	Reference No.
1	Mmouse anti-NeuN	IHC	Millipore Sigma	MAB377
2	Anti-Iba1	IHC	Wako Laboratory	019-19741
3	Mouse anti-rat CD4	IHC	ebioscience	14-0040-82
4	Mouse anti-rat CD68:Alexa Fluor 647	FC	Bio-Rad	mca341a647
6	Mouse anti-rat CD5:Alexa Fluor 647	FC	Bio-Rad	mca52a647
7	Mouse anti-rat CD8 ALPHA:Alexa Fluor 647	FC	Bio-Rad	mca48a647
8	Anti-Mouse/Rat CD90.1 (Thy-1.1) PerCP-Cyanine5.5	FC	ebioscience	45-0900-80
9	Mouse anti-rat CD25:RPE	FC	Bio-Rad	mca273pe
10	Mouse anti-rat CD3:Alexa Fluor 647	FC	Bio-Rad	mca772a647
11	Anti-Rat CD45 FITC, OXO1	FC	ebioscience	11-0461-82
13	Anti-Mouse/Rat IL-17A Alexa Fluor 488	FC	ebioscience	537177-81
14	Mouse anti-rat CD68:RPE	FC	Bio-Rad	mca341pe
15	Mouse anti-rat CD4 647	FC	Bio-Rad	mca55ga

FC, flow cytometry; IHC, immunohistochemistry.

Table 2. *Real-time PCR primers in the rat*

Assay ID	Abbreviated Name	Full Name	Vendor	Type
Rn00562488_s1	Adra2a	Adrenoceptor-α2A	ThermoFisher	TaqMan
Rn00593312_s1	Adra2b	Adrenoceptor-α2B	ThermoFisher	TaqMan
Rn00593341_s1	Adra2c	Adrenoceptor-α2C	ThermoFisher	TaqMan
Rn00824536_s1	Adrb1	Adrenoceptor-β1	ThermoFisher	TaqMan
Rn00560650_s1	Adrb2	Adrenoceptor-β2	ThermoFisher	TaqMan
Rn00580555_m1	Ccl2	chemokine (C-C motif) ligand 2	ThermoFisher	TaqMan
Rn01637698_s1	Ccr2	chemokine (C-C motif) receptor 2	ThermoFisher	TaqMan
Rn01472831_m1	Hifla	hypoxia-inducible factor 1, α-subunit	ThermoFisher	TaqMan
Rn00709342_m1	Itgam	integrin, α-M	ThermoFisher	TaqMan
Rn00569848_m1	Tlr4	Toll-like receptor 4	ThermoFisher	TaqMan

E-5200) according to the manufacturer's protocol. The ELISA plates were evaluated spectrophotometrically at 450 nm (SynergyMx multimode microplate reader, Biotek). The quantification of NE content was achieved by comparing its absorbance with a reference curve prepared with a known standard concentration, as per manufacturer's protocol. All samples were run in duplicates. The NE content was normalized for total protein level in the BM. The protein concentration of BM supernatant was determined by Bio-Rad protein assay method following the manufacturer's instruction.

Statistical analyses. Results were expressed as the means ± SE and analyzed using either two-tailed Student's *t*-test (when only two groups were compared) or a one-way ANOVA when appropriate, using GraphPad Prism (GraphPad Software, La Jolla, CA). The level of significance was established at $P < 0.05$ and denoted in each figure.

RESULTS

In situ electrophysiology and in vivo radiotelemetry reveal ANG II-dependent shifts in fSNA associated with blood pressure increase. We used DAPR (schematics in Fig. 1*A*) to determine effects of intracerebroventricular ANG II on fSNA over time. Integrated fSNA (control, *day 3* and *day 7*) was averaged over 100 phrenic cycles to determine its activity patterns within different stages of PNA: inspiratory/postinspiratory (I/P-I) and expiratory (E) stage, as previously described (35). We observed a significant shift in the fSNA peak activity from the typical peak in the I/P-I phase to E phase of PNA cycle at *day 7* (Fig. 1*A*, *middle*, arrow shows the increase in fSNA amplitude in E stage). This shift in peak fSNA was quantified by comparing relative amplitude peaks at I/P-I versus E stages between *day 3* and *day 7* and their appropriate control (Fig. 1*B*). We observed increased amplitude peaks of fSNA in the E stage and decreased ones in the I/P-I stage at *day 7* but not *day 3* of intracerebroventricular ANG II infusion (Fig. 1*A*, *top right*, triangle shapes). These patterns were typical of the sympathetic respiratory uncoupling previously reported in hypertensive rats, suggestive of HTN-associated changes in the sympathetic drive (34, 35). BM SNAX significantly decreased NE levels in the femoral BM of rats at *day 7* of ANG II infusion compared with SHAM BM in same rats (Fig. 1*A*, *bottom right*, $P < 0.05$), confirming that 7 days of intracerebroventricular ANG II infusion increases NE levels in the femur via fSNA. Radiotelemetry recordings in conscious, freely moving rats revealed a significant increase in MBP and SBP at *day 7* and *day 14* of intracerebroventricular ANG II infusion, respectively (Fig. 1*B*). This suggests that increase in fSNA at *day 7* parallels the development of high BP in this model.

Elevated bone marrow and systemic inflammatory factors correlate with ANG II-dependent elevation in fSNA. Corresponding with the timing of elevated fSNA and MBP at *day 7* of intracerebroventricular ANG II infusion, we observed a significant increase in $CD4^+.IL17^+$ ICs in blood and BM at *day 7* of intracerebroventricular ANG II infusion (Fig. 2*B*, $P < 0.05$). Figure 2*A* illustrates a typical increase in blood $CD4^+.IL17^+$ ICs from control to *day 7* of intracerebroventricular ANG II infusion. Additionally, we found a significant elevation in $CD90^+.CD4.5.8^-$ angiogenic progenitor cells in the blood, and elevation in several other T cell subtypes as well as $CD68^+$ macrophages in the BM at *day 7* of intracerebroventricular ANG II infusion (Fig. 2*B*, $P < 0.05$). Similarly, several inflammatory markers were significantly elevated (e.g., CCL2, HIF1a, and ITGAM, $P < 0.05$) at *day 7* compared with control (Fig. 2*D*). Interestingly, reduced inflammatory markers in blood and BM by *day 21* compared with *day 7* of intracerebroventricular ANG II infusion (Fig. 1, *B–D*), despite the continuous SBP and MBP increase, suggest possible clearance from circulation and tissue infiltration. Furthermore, we observed a significant reduction in several T cell subtypes ($CD4^+.IL17^+$, $CD4^+.CD25^+$, and $CD3^+$ T cells) following BM SNAX versus SHAM at *day 7* of intracerebroventricular ANG II infusion (Fig. 1*C*, $P < 0.05$). Moreover, relative expression levels of several inflammatory markers (CCL2, CCR2, HIF1a, and ITGAM) were also significantly decreased in the BM following BM SNAX at *day 7* (Fig. 1*D*, *left*, $P < 0.05$). Finally, using PCR we determined a significant increase in Adrb1, Adra2a, and Adra2b relative expression levels at *day 21* of intracerebroventricular ANG II infusion, whereas BM SNAX at *day 7* reduced the levels of Adra2a, Adra2b, and Adra2c (Fig. 2*D*, *right*, $P < 0.05$). Thus, it appears that levels of several inflammatory cells and markers in BM and blood are dependent on fSNA increase at *day 7* of intracerebroventricular ANG II infusion and therefore elevate prior to or in parallel with ANG II-dependent rise in BP.

Activation of microglia characterizes early stages of rodent HTN, whereas infiltration of peripheral $CD4^+$ cells corresponds to the timing of established rodent ANG II HTN. Our previous study showed an increased proportion of activated microglia in the PVN 1 h after a single ANG II challenge, which persisted after BP normalization (37). However, it is unknown whether microglial activation precedes the onset of peripheral inflammation or alterations in BP. Thus, the next objective was to determine when the microglial activation occurred in response to intracerebroventricular ANG II. Figure

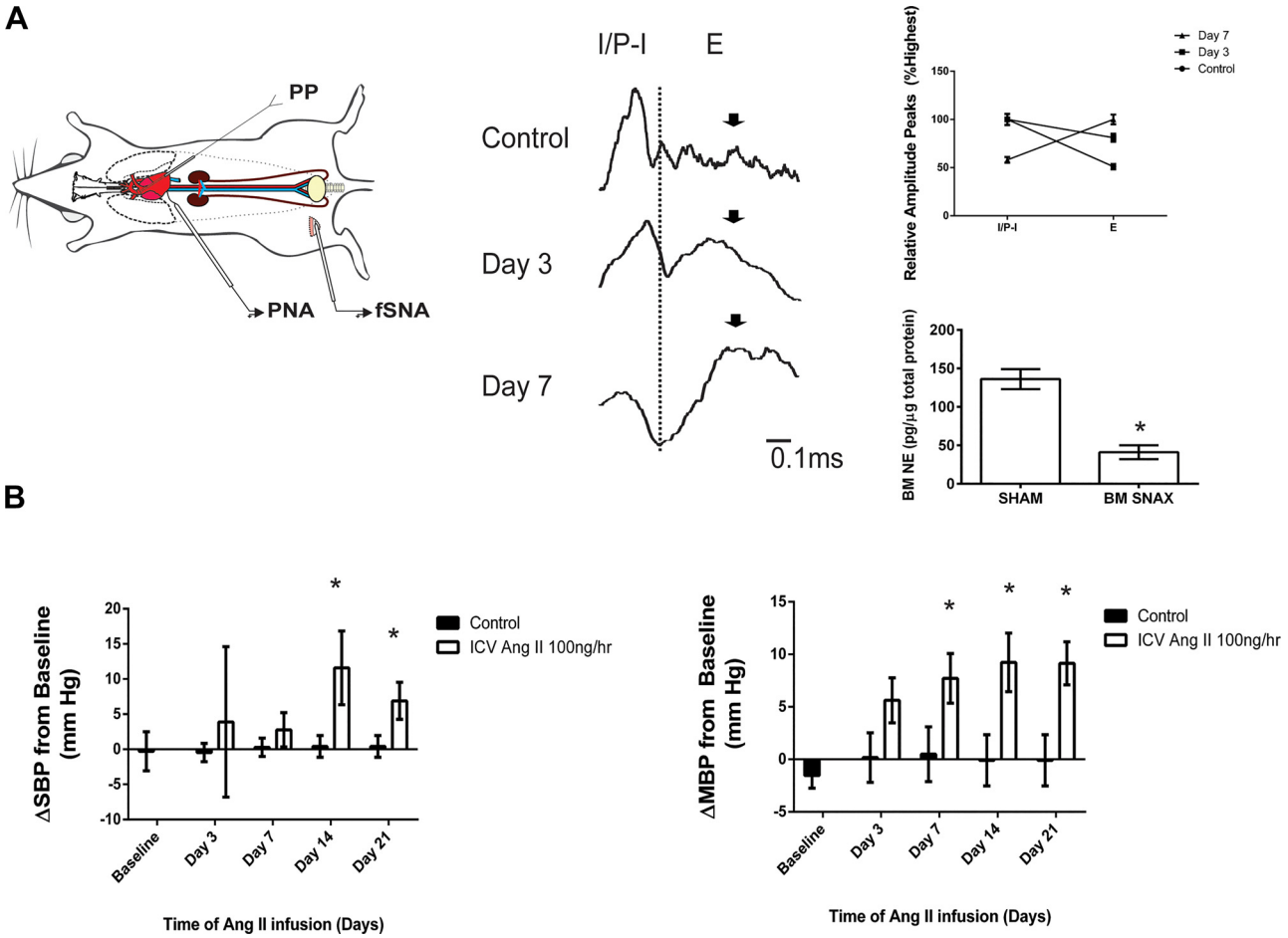

Fig. 1. Centrally administered ANG II is associated with elevated femoral sympathetic nerve activity (fSNA) and blood pressure (BP) in rats. *A*: in situ electrophysiology revealed a shift in the fSNA peak activity from the typical inspiratory/postinspiratory (I/P-I) phase to the expiratory (E) phase, suggesting sympathetic respiratory uncoupling typical of that seen in rodent models of hypertension. *Left*: a schematic of decerebrated artificially perfused rat preparation used to record the activity of fSNA and phrenic nerve activity (PNA) in situ. *Middle*: shift in the peak of fSNA activity to E phase of the respiratory cycle (arrow) that begins as early as *day 3* of intracerebroventricular (ICV) ANG II infusion and elevates at *day 7*. *Right*: a marked shift in the peak fSNA from I/P-I to E at *day 7* (top graph) and protein levels of bone marrow (BM) norepinephrine (NE) in sympathetic nerve denervated femur (BM SNAX) compared with SHAM femur in rats at *day 7* of ICV ANG II infusion (bottom graph). *B*: significantly increased systolic blood pressure (SBP) at *day 14* (*left*) and mean blood pressure (MBP) at *day 7* (*right*) of ICV ANG II infusion. PP, perfusion pressure. Data are presented as means ± SE, $n = 6$ rats; *$P < 0.05$ vs. control, ANOVA or *t*-test where applicable.

3 illustrates microglial activation and morphology in rats that were chronically infused with intracerebroventricular ACSF (control) or intracerebroventricular ANG II (100 ng/h) for 3, 7, and 21 days. Image acquisition and immunolabeling were optimized to determine changes in microglial activation state in the PVN. Three coronal sections from each animal were mounted on a glass slide and labeled with anti-Iba1 (Fig. 3*B*). Confocal microscopy was used to capture and stitch a single high-definition image of the entire PVN (Fig. 3*B*), and image processing was carried out to validate changes in microglial morphology. Microglial activation is marked by a change from ramified/resting state characterized by smaller cell bodies and extensive branching of cellular processes to an activated ameboidal state characterized by larger cell bodies, loss of branched processes, and increased reactivity with Iba1 (as represented in Fig. 3*B*, *bottom*). Congruent with our previous findings (37), we observed a distinct change in microglial activation in the PVN in response to ANG II infusion as confirmed by manual count of Iba1$^+$ cells in the PVN and circularity index (a quantitative measure of cell complexity) (Fig. 3, *A* and *B*). Notably, circularity assessment of Iba1$^+$ cells in the PVN indicates that microglial activation occurs as early as after 3 days of intracerebroventricular ANG II infusion (Fig. 3*A*). Reactive microglia have a circularity higher than resting or ramified microglia due to the loss of extensive, branched processes and increase in cell body size. This suggested a significant change in microglial morphology in the PVN early in the ANG II infusion timeline, i.e., at *day 3*. Although the change in morphology occurred at 3 days of ANG II infusion (Fig. 3*A*, *left* and Fig. 3*B*, *bottom*), increase in microglial cell population was seen from *days 7–21* of ANG II infusion (Fig. 3*A*, *right*, $P < 0.05$). As Iba1 is a marker for both peripheral macrophages and central nervous system microglial cells, it is unclear whether the increase in Iba1$^+$ cells in the PVN is due to resident microglial mitosis or infiltration of peripheral cells. Therefore, we next explored whether chronic ANG II infusion is associated with an increase in infiltration of peripheral immune cells. At 21 days of intracerebroventricular ANG II infusion, characterized by established HTN (as in Fig. 1),

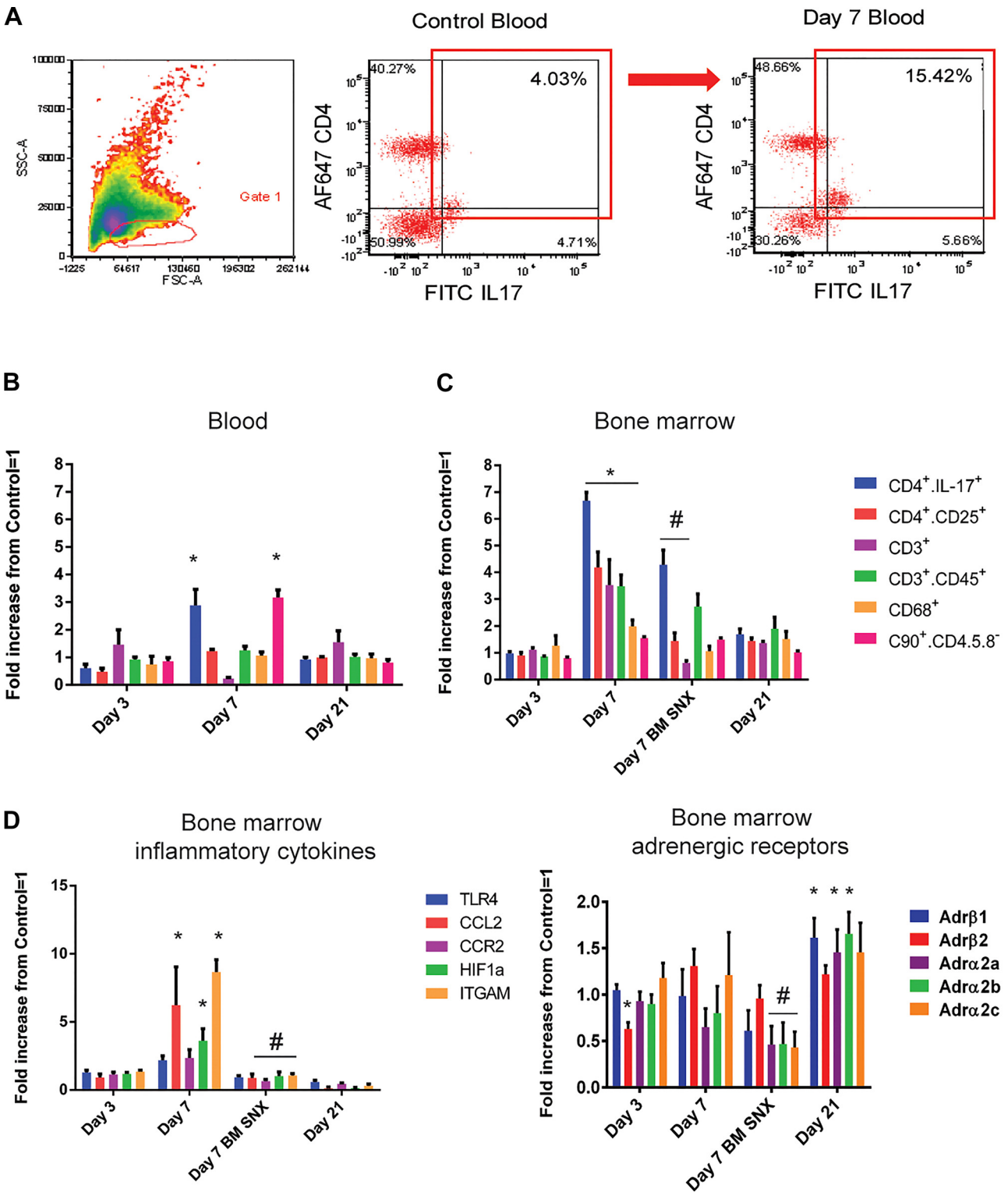

Fig. 2. Central administration of ANG II is associated with elevated bone marrow (BM) and circulating inflammatory markers. Intracerebroventricular (ICV) ANG II increased levels of $CD4^+.IL17^+$ T cells in the blood (*A* and *B*) and BM (*C*) at *day 7*, as measured by flow cytometry. In addition, levels of several other T cell subtypes ($CD4^+.CD25^+$, $CD3^+$, $CD3^+.CD45^+$, and $CD68^+$ macrophage/monocytes were increased in the BM at *day 7* of ANG II infusion (*C*), as measured by flow cytometry. Dennervation of the femoral BM sympathetic nerve (BM SNX) at *day 7* of ICV ANG II infusion significantly reduced the ANG II-dependent increase in the inflammatory cells in the BM (*C*), suggesting BM sympathetic nerve activity-dependent activation of BM immune system by ANG II, as measured by flow cytometry. Real-time PCR showed elevated levels of several inflammatory markers, including TLR4, HIF1a, and ITGAM, in the BM at *day 7* of ANG II infusion (*D*), which was reduced by BM SNX (*left*); significant elevation in several adrenergic receptors in the BM at *day 21* of ANG II infusion, as measured by real-time PCR (*right*). Data are presented as means ± SE, $n = 6$; *$P < 0.05$ vs. control; #$P < 0.05$ vs. *day 7*; ANOVA.

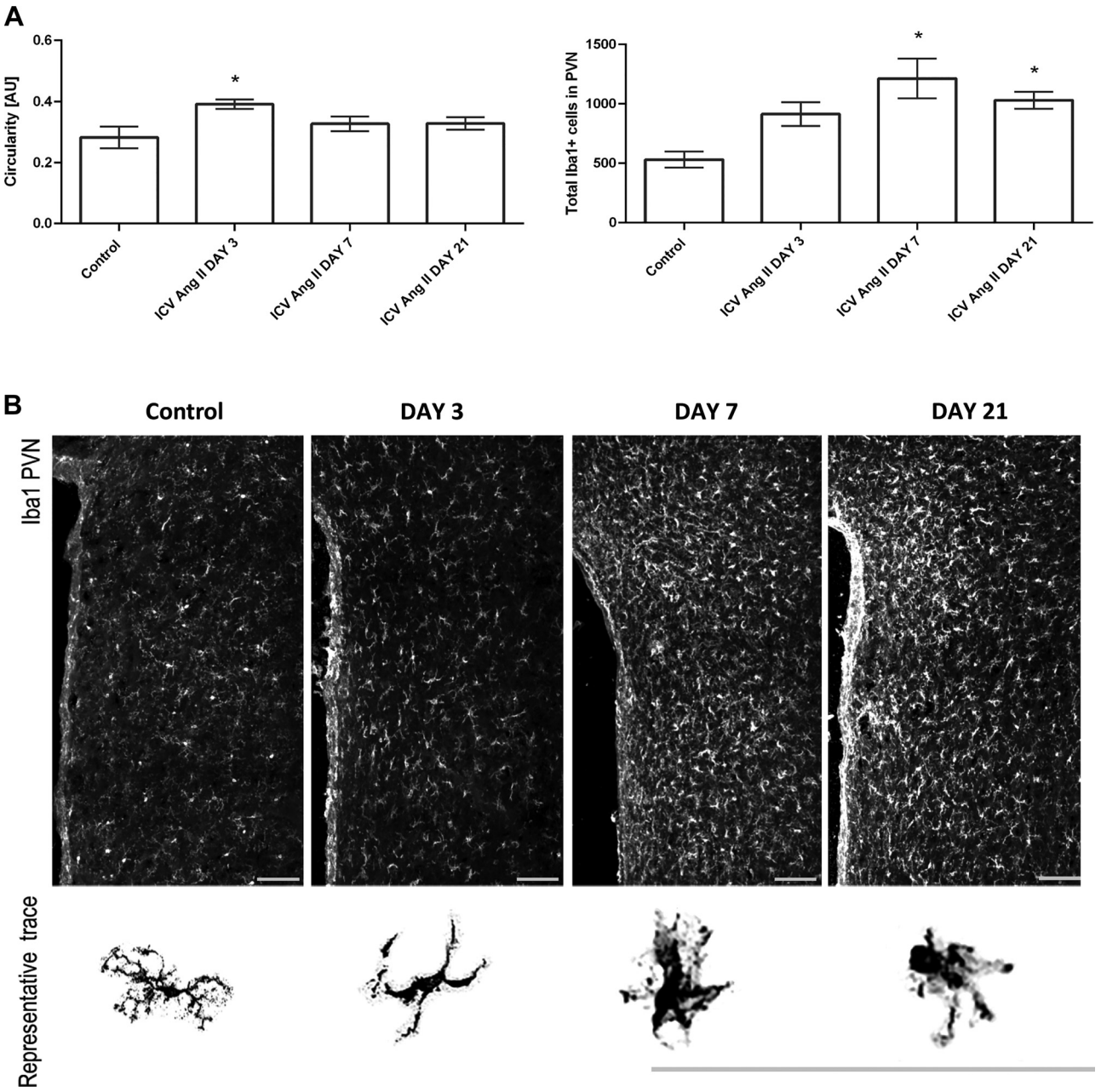

Fig. 3. Intracerebroventricular (ICV) administration of ANG II for 3, 7, and 21 days produced graded, time-dependent neuroinflammatory responses in the paraventricular nucleus (PVN) of rats, as evident by microglial morphology and Iba1-positive cell count. *A* (*left*): binary masks were used to quantify circular morphology of Iba1$^+$ cells in the PVN of all rats (as represented in *B*, *bottom*). Mathematical quantification of cell circularity indicates a change in microglial activation at *day 3* of ICV ANG II infusion. Circularity was calculated based on the area and perimeter of each Iba1$^+$ cell and represents shortening of cell processes and thickening of cell bodies (as represented in *B*, *bottom*), both properties indicative of microglial activation. *A* (*right*): quantification of total number of nucleated Iba1$^+$ cells in the PVN shows a significant increase at *days 7* and *21* of ANG II compared with control. *B*: representative confocal images of rat PVN slices immunolabeled with Iba1 (white) reveal a progressive increase in Iba1$^+$ cells with ANG II infusion. Data are presented as means ± SE, $n = 6$ rats. *$P < 0.05$ vs. control, ANOVA.

we observed infiltration of CD4$^+$ cells into the PVN (Fig. 4*A*). For this analysis, all nucleated cells robustly positive for CD4, which matched morphological characteristics of T cells described in the literature (and exemplified in Fig. 4*C*) (7, 20), were manually counted by two independent researchers, and total cell counts were plotted (Fig. 4*D*). At 21 days of ANG II infusion, we observed a significant increase in the number of CD4$^+$ cells in the PVN (Fig. 4*D*, $P < 0.05$). High-magnification confocal microscopy also revealed colocalization of microglia (Iba1, in green) and CD4 (in red), as well as neuronal cells (NeuN, in green) and CD4 (in red) in the PVN at *day 21* of intracerebroventricular ANG II infusion (Fig. 4*B*); however, these changes were not quantified.

DISCUSSION

Interplay between the ANS and IS has recently become of great interest in the HTN field. Others have shown a direct link between renal denervation and reduced inflammation in the

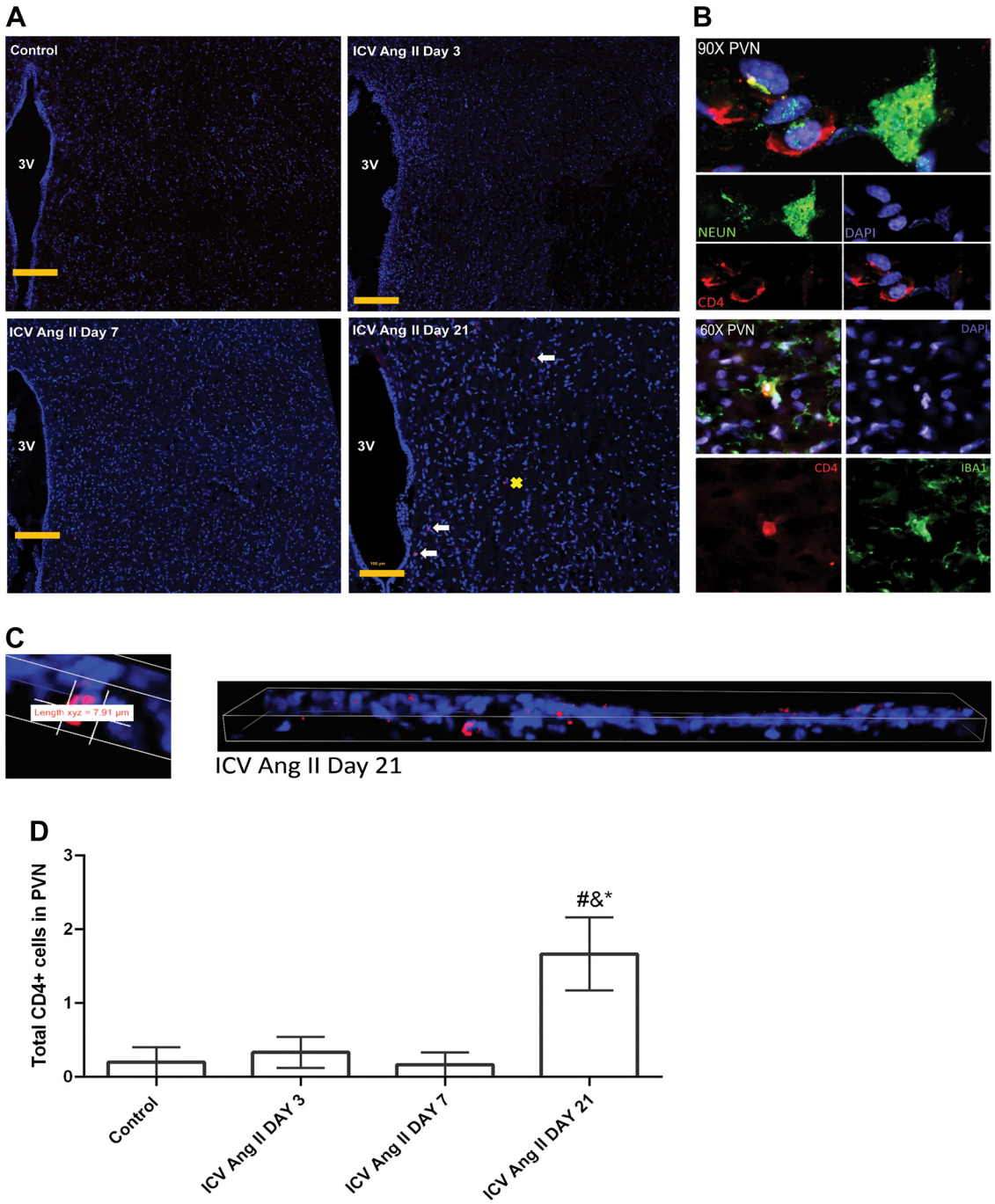

Fig. 4. Increased presence of CD4-positive cells in the paraventricular nucleus (PVN) at *day 21* of intracerebroventricular (ICV) ANG II infusion. *A*: representative confocal images of immunolabeling for CD4 (red) counterstained with DAPI (blue) in the PVN at *days 3*, *7*, and *21* following continuous infusion of ANG II (100 ng/h icv) or artificial cerebrospinal fluid (control). White arrows point to the cells counted as CD4-positive cells, which were identified as round nucleated cells present in both the max intensity and three-dimensional projection of each image with their whole length ranging from 6–8 μm (as depicted in *C* below). Yellow cross marks the apparent positive label that was excluded from the total CD4-positive cell count as per our stringent exclusion methods. The position of the third ventricle (3V) is marked. *B*: high-magnification confocal microscopy illustrates the proximity of CD4-positive cells to neurons (*top* at ×90: NeuN in green, CD4 in red, DAPI in blue) and microglia (*bottom* at ×60: Iba1 in green, CD4 in red, DAPI in blue) in the PVN at *day 21* of ANG II infusion. *D*: quantification of CD4-positive cells shows a statistically significant increase in CD4-positive cells in the PVN at *day 21* of ANG II infusion only. Data are presented as means ± SE, $n = 5$ rats; $^*P < 0.05$ vs. control, $\#P < 0.05$ vs. *day 3*, $\&P < 0.05$ vs. *day 7*, ANOVA.

denervated kidney (27), possibly via direct effect of NE on ICs such as T cells and dendritic cells (12), shown to be important in HTN (3, 12, 27, 35). We chose to investigate the role of the BM in HTN, as the main hematopoietic organ in the body, and in view of our previous study that suggested an associative link between elevated BM fSNA and exaggerated IS in the spontaneously hypertensive rat (SHR) (35). Conversely, genetic ablation of BM adrenergic β-receptors produced overall immunosuppression and lowered BP in a novel mouse chimera model (2), confirming a close association between the SNA, IS,

and HTN. Moreover, we observed reduced infiltration of peripheral ICs and significant downregulation of IS networks in the gut of these mice, suggesting that reduced systemic inflammation translated to reduced local tissue inflammation and underscoring a functional significance of the ANS-IS axis in control of BP (30). Infiltration of peripheral ICs has been reported in many tissues in HTN, including the brain (11, 13, 21, 22). In the brain, increased infiltration of peripheral BM-derived ICs to the PVN is shown in later stages of ANG II-dependent HTN and in a chimera model in which the BM cells from the SHR were fully reconstituted (21). In the latter study, an increase in BP following reconstitution with SHR BM cells is associated with neuroinflammation and elevated sympathetic drive (21), suggesting that IC infiltration can affect neuronal activity in the presympathetic brain regions. However, studies to date have only confirmed presence of the infiltrating ICs in the brain cardioregulatory regions in the late stages of established HTN. Here, we investigated a temporal relationship between central ANG II, activation of central and peripheral IS, BM fSNA, and elevation of BP to investigate a cause-effect relationship in early and established stages of neurogenic HTN. To achieve this, we used a central infusion of a low dose of ANG II that would elevate BP at a slower rate and thus allow temporal separation of the effects on SNA, BP, and inflammation and allude to possible cause-effect relationships.

Our present study uncovers several novel findings: (*1*) We observed a significant ANG II-dependent neuroinflammation in the PVN, characterized by activation (i.e., reduced circularity) of resident microglia as early as *day 3* of ANG II infusion, and before the increase in both fSNA and BP; (*2*) shifts in fSNA at *day 7* of ANG II infusion correlate with the timing of elevated BM inflammatory markers and release of ICs into the circulation, the timeline of which also coincides with early elevation of BP; and (*3*) late-stage HTN is marked by infiltration of $CD4^+$ T cells in the PVN. Thus, our data suggest a role for activated microglia in modulation of PVN neuronal responses, leading to increased sympathetic drive to the BM, which activates the peripheral IS early in HTN. Subsequent infiltration of continuously activated ICs from the periphery to the brain may further exacerbate neuroinflammatory responses in the PVN in established HTN.

Activation of microglia is a hallmark of rodent models of neurogenic HTN. It is unclear, however, whether microglia can respond to ANG II directly, or only following microglial activation (25) (8). As we observe early activation of microglia following intracerebroventricular ANG II administration, it is possible that this may be a consequence of enhanced central neuro-glial communication, as neurons are able to respond to ANG II (9), rather than the direct effects of ANG II on microglia. Indeed, this phenomenon has been previously described in other models of neurologic diseases (26), in which microglia are reacting to the distress call from neurons by mobilizing and activating to promote neuronal survival. Thus, continued presence of centrally administered ANG II leading to activation of presympathetic neurons may inadvertently be responsible for early neuroinflammatory responses in the PVN. Future studies should address these questions more specifically.

The early microglial activation in the PVN precedes activation of the BM fSNA, suggesting causation. Using retrograde tracing, we have previously shown a direct neural communication between the BM and the brain cardioregulatory regions (16) that appears to be enhanced in the SHR and ANG II rodent HTN (35). In the present study, the activation of BM fSNA is associated with elevated production of BM inflammatory markers and ICs, including the $CD4^+.IL17^+$ T cells associated with HTN and immune disorders (17, 24, 37). The fSNA-dependent mobilization of these cells into circulation may have an important role in early stages of ANG II HTN, due to their reportedly elevated tissue-invading ability as well as the ability to break down the blood brain barrier (14). Indeed, the elevated presence of $CD4^+.IL17^+$ T cells in circulation is associated with initiation of BP pressure responses in early stages of ANG II HTN in the present study, whereas a single injection of ANG II has shown to elevate levels of these cells in circulation of rats (37). Most interestingly, PVN infiltration of $CD4^+$ T cells was observed at *day 21* of ANG II infusion in the present study. Consequently, we observed lower levels of circulating $CD4^+.IL17^+$ at *day 21* compared with *day 7* of ANG II infusion, suggesting their clearance from circulation and a tissue-infiltrating trait that progresses with HTN. The relatively low number of $CD4^+$ peripheral cells that infiltrate the PVN at *day 21* of ANG II infusion is by no means dismissive of their importance in the context of HTN and other conditions (21, 28, 29); however, further studies are needed to elucidate their precise role in the PVN upon infiltrating to close this gap in knowledge.

In addition to $CD4^+.IL17^+$ cells, there is a significant elevation in $CD90^+.CD4.5.8^-$ angiogenic progenitor cells in the blood but not the BM at *day 7*, whereas BM denervation did not affect the levels of these cells in the BM at *day 7*. Thus, it appears that these cells are not directly controlled by the fSNA, which was also shown in our mouse model with chronic genetic ablation of adrenergic receptors (2, 31). Thus, their increase in the blood at *day 7* may not be due to increased BM fSNA, but it may be due to other factors. Indeed, one role of angiogenic progenitor cells is repair of vascular and tissue damage (32), as increase in BP at *day 7* is a possible beginning to cause this damage. Additionally, elevation in several other T cell subtypes and $CD68^+$ macrophages were observed in the BM at *day 7* of intracerebroventricular ANG II infusion, whereas BM SNAX only significantly affected the levels of specific T cells in the BM at *day 7*. This is an interesting observation and in line with other recent studies showing direct effects of NE on different T cell subtypes (27, 38). It may also mean that the timeline for fSNA-driven activation of macrophages, for example, may be longer than 7 days or that it indeed requires other factors such as circulating ANG II to produce the full inflammatory effect. Further studies are needed to delineate this.

There appeared to be an increase in BP at *day 3* of intracerebroventricular ANG II infusion; however, this was not statistically significant. We did not measure the overall vasomotor sympathetic drive, but it is possible that the activation of microglia at *day 3* would also begin to elevate the overall vasomotor and renal sympathetic drive, which would account for the apparent but not statistically significant BP changes observed at *day 3*. However, this was beyond the scope of the study, as our main goal was to temporally correlate changes in specific BM fSNA with IS and BP responses. Considering the appropriate sample used, we are confident in the statistical

power of our current study and that it indeed shows the timeline of BP increase in this model.

An interesting observation is that relative expression levels of several adrenergic receptors on BM ICs are increased at *day 21* following intracerebroventricular ANG II infusion, which is a delayed effect compared with the onset of ANG II-dependent shifts in fSNA, IS, and BP. Conversely, BM SNAX reduced relative expression levels of some but not all these receptors while chronic genetic ablation of β-adrenergic receptors caused a significant drop in BP that is associated with a reduction in the levels of circulating ICs, including the $CD4^+$ T cells (1, 30). Thus, it appears that the timeline of adrenergic receptor expression following continuous receptor activation versus inactivation may differ between the specific receptors, which could be relevant for antihypertensive therapy that includes adrenergic receptor blockers. For example, it appears that early activation of Adrβ1 at *day 7* does not increase the relative expression levels of this receptor on BM ICs; however, administration of β blockers earlier in developing HTN may lower inflammatory profiles at later stages by preventing overexpression of these receptors possibly caused by overstimulation via fSNA. Further studies are needed to investigate this.

We show that ANG II HTN in our model is marked by early neuroinflammatory responses preceding the increase in fSNA and BP, whereas late stage HTN follows the fSNA-dependent activation and infiltration of BM-derived ICs. Blockade of BM IC and especially $CD4^+$ T cell infiltration into the brain regions relevant in cardiovascular control may present an important avenue to explore in neurogenic HTN therapeutics (18). Further studies are required to elucidate precise molecular and cellular mechanisms of the neuro-immune interactions in the brain, but this opens up novel therapeutic avenues for not only HTN, but also many other central nervous system diseases associated with IS dysfunction.

ACKNOWLEDGMENTS

We thank Joseph Leibowitz and Dr. W. J. Streit from University of Florida for their valuable input and expertise.

GRANTS

This work was supported by American Heart Association Grant 14SDG18300010 (to J. Zubcevic) and National Heart, Blood, and Lung Institute Grants T32-HL-083810 (to N. Ahmari) and R56-HL-136692-01 (to J. Zubcevic).

DISCLOSURES

No conflicts of interest, financial or otherwise, are declared by the authors.

AUTHOR CONTRIBUTIONS

N.A., H.K., D.M.B., M.K.R., and J.Z. conceived and designed research; N.A., M.M.S., N.M.G., R.L., T.L.R., H.D., H.K., D.M.B., M.K.R., and J.Z. performed experiments; N.A., M.M.S., D.R.M., N.M.G., R.L., T.L.R., H.D., H.K., D.M.B., M.K.R., and J.Z. analyzed data; N.A., M.M.S., D.R.M., N.M.G., R.L., T.L.R., H.D., H.K., D.M.B., M.K.R., and J.Z. interpreted results of experiments; N.A., M.M.S., D.R.M., R.L., H.D., H.K., D.M.B., M.K.R., and J.Z. prepared figures; N.A., M.K.R., and J.Z. drafted manuscript; N.A., D.M.B., M.K.R., and J.Z. edited and revised manuscript; N.A., M.M.S., D.R.M., N.M.G., R.L., T.L.R., H.D., H.K., D.M.B., M.K.R., and J.Z. approved final version of manuscript.

REFERENCES

1. **Ahmari N, Santisteban M, Baekey D, Raizada M, Zubcevic J.** Angiotensin II–dependent increase in the b=bone marrow sympathetic drive initiates the inflammatory and endothelial progenitor cell imbalance and precedes blood pressure increase (Abstract). *FASEB J* 29, *Suppl* 1: 1059.1, 2015.
2. **Ahmari N, Schmidt JT, Krane GA, Malphurs W, Cunningham BE, Owen JL, Martyniuk CJ, Zubcevic J.** Loss of bone marrow adrenergic beta 1 and 2 receptors modifies transcriptional networks, reduces circulating inflammatory factors, and regulates blood pressure. *Physiol Genomics* 48: 526–536, 2016. doi:10.1152/physiolgenomics.00039.2016.
3. **Case AJ, Roessner CT, Tian J, Zimmerman MC.** Mitochondrial superoxide signaling contributes to norepinephrine-mediated t-lymphocyte cytokine profiles. *PLoS One* 11: e0164609, 2016. doi:10.1371/journal.pone.0164609.
4. **Centenera MM, Selth LA, Ebrahimie E, Butler LM, Tilley WD.** New opportunities for targeting the androgen receptor in prostate cancer. *Cold Spring Harb Perspect Med* 8: a030478, 2018. doi:10.1101/cshperspect.a030478.
5. **Chi DS, Harris NS.** A simple method for the isolation of murine peripheral blood lymphocytes. *J Immunol Methods* 19: 169–172, 1978. doi:10.1016/0022-1759(78)90176-X.
6. **Cooper ST, Sell SS, Fahrenkrog M, Wilkinson K, Howard DR, Bergen H, Cruz E, Cash SE, Andrews MT, Hampton M.** Effects of hibernation on bone marrow transcriptome in thirteen-lined ground squirrels. *Physiol Genomics* 48: 513–525, 2016. doi:10.1152/physiolgenomics.00120.2015.
7. **D'Agostino PM, Gottfried-Blackmore A, Anandasabapathy N, Bulloch K.** Brain dendritic cells: biology and pathology. *Acta Neuropathol* 124: 599–614, 2012. doi:10.1007/s00401-012-1018-0.
8. **de Kloet AD, Liu M, Rodríguez V, Krause EG, Sumners C.** Role of neurons and glia in the CNS actions of the renin-angiotensin system in cardiovascular control. *Am J Physiol Regul Integr Comp Physiol* 309: R444–R458, 2015. doi:10.1152/ajpregu.00078.2015.
9. **de Kloet AD, Pati D, Wang L, Hiller H, Sumners C, Frazier CJ, Seeley RJ, Herman JP, Woods SC, Krause EG.** Angiotensin type 1a receptors in the paraventricular nucleus of the hypothalamus protect against diet-induced obesity. *J Neurosci* 33: 4825–4833, 2013. doi:10.1523/JNEUROSCI.3806-12.2013.
10. **Dutta P, Sager HB, Stengel KR, Naxerova K, Courties G, Saez B, Silberstein L, Heidt T, Sebas M, Sun Y, Wojtkiewicz G, Feruglio PF, King K, Baker JN, van der Laan AM, Borodovsky A, Fitzgerald K, Hulsmans M, Hoyer F, Iwamoto Y, Vinegoni C, Brown D, Di Carli M, Libby P, Hiebert SW, Scadden DT, Swirski FK, Weissleder R, Nahrendorf M.** Myocardial infarction activates $CCR2^+$ hematopoietic stem and progenitor cells. *Cell Stem Cell* 16: 477–487, 2015. doi:10.1016/j.stem.2015.04.008.
11. **Gauthier M, Chakraborty K, Oriss TB, Raundhal M, Das S, Chen J, Huff R, Sinha A, Fajt M, Ray P, Wenzel SE, Ray A.** Severe asthma in humans and mouse model suggests a CXCL10 signature underlies corticosteroid-resistant Th1 bias. *JCI Insight* 2: e95480, 2017. doi:10.1172/jci.insight.94580.
12. **Guzik TJ, Hoch NE, Brown KA, McCann LA, Rahman A, Dikalov S, Goronzy J, Weyand C, Harrison DG.** Role of the T cell in the genesis of angiotensin II induced hypertension and vascular dysfunction. *J Exp Med* 204: 2449–2460, 2007. doi:10.1084/jem.20070657.
13. **Guzik TJ, Skiba DS, Touyz RM, Harrison DG.** The role of infiltrating immune cells in dysfunctional adipose tissue. *Cardiovasc Res* 113: 1009–1023, 2017. doi:10.1093/cvr/cvx108.
14. **Huppert J, Closhen D, Croxford A, White R, Kulig P, Pietrowski E, Bechmann I, Becher B, Luhmann HJ, Waisman A, Kuhlmann CR.** Cellular mechanisms of IL-17-induced blood-brain barrier disruption. *FASEB J* 24: 1023–1034, 2010. doi:10.1096/fj.09-141978.
15. **Itani HA, McMaster WG Jr, Saleh MA, Nazarewicz RR, Mikolajczyk TP, Kaszuba AM, Konior A, Prejbisz A, Januszewicz A, Norlander AE, Chen W, Bonami RH, Marshall AF, Poffenberger G, Weyand CM, Madhur MS, Moore DJ, Harrison DG, Guzik TJ.** Activation of human T cells in hypertension: studies of humanized mice and hypertensive humans. *Hypertension* 68: 123–132, 2016. doi:10.1161/HYPERTENSIONAHA.116.07237.
16. **Jun JY, Zubcevic J, Qi Y, Afzal A, Carvajal JM, Thinschmidt JS, Grant MB, Mocco J, Raizada MK.** Brain-mediated dysregulation of the bone marrow activity in angiotensin II-induced hypertension. *Hypertension* 60: 1316–1323, 2012. doi:10.1161/HYPERTENSIONAHA.112.199547.
17. **Kim S, Goel R, Kumar A, Qi Y, Lobaton G, Hosaka K, Mohammed M, Handberg EM, Richards EM, Pepine CJ, Raizada MK.** Imbalance of gut microbiome and intestinal epithelial barrier dysfunction in patients

with high blood pressure. *Clin Sci (Lond)* 132: 701–718, 2018. doi:10.1042/CS20180087.

18. **Oh YS, Appel LJ, Galis ZS, Hafler DA, He J, Hernandez AL, Joe B, Karumanchi SA, Maric-Bilkan C, Mattson D, Mehta NN, Randolph G, Ryan M, Sandberg K, Titze J, Tolunay E, Toney GM, Harrison DG.** National heart, lung, and blood institute working group report on salt in human health and sickness: building on the current scientific evidence. *Hypertension* 68: 281–288, 2016. doi:10.1161/HYPERTENSIONAHA.116.07415.
19. **Ohsaki A, Venturelli N, Buccigrosso TM, Osganian SK, Lee J, Blumberg RS, Oyoshi MK.** Maternal IgG immune complexes induce food allergen-specific tolerance in offspring. *J Exp Med* 215: 91–113, 2018. doi:10.1084/jem.20171163.
20. **Rasouli J, Ciric B, Imitola J, Gonnella P, Hwang D, Mahajan K, Mari ER, Safavi F, Leist TP, Zhang GX, Rostami A.** Expression of GM-CSF in T cells is increased in multiple sclerosis and suppressed by IFN-β therapy. *J Immunol* 194: 5085–5093, 2015. doi:10.4049/jimmunol.1403243.
21. **Santisteban MM, Ahmari N, Carvajal JM, Zingler MB, Qi Y, Kim S, Joseph J, Garcia-Pereira F, Johnson RD, Shenoy V, Raizada MK, Zubcevic J.** Involvement of bone marrow cells and neuroinflammation in hypertension. *Circ Res* 117: 178–191, 2015. doi:10.1161/CIRCRESAHA.117.305853.
22. **Santisteban MM, Qi Y, Zubcevic J, Kim S, Yang T, Shenoy V, Cole-Jeffrey CT, Lobaton GO, Stewart DC, Rubiano A, Simmons CS, Garcia-Pereira F, Johnson RD, Pepine CJ, Raizada MK.** Hypertension-linked pathophysiological alterations in the Gut. *Circ Res* 120: 312–323, 2017. doi:10.1161/CIRCRESAHA.116.309006.
23. **Tzartos JS, Friese MA, Craner MJ, Palace J, Newcombe J, Esiri MM, Fugger L.** Interleukin-17 production in central nervous system-infiltrating T cells and glial cells is associated with active disease in multiple sclerosis. *Am J Pathol* 172: 146–155, 2008. doi:10.2353/ajpath.2008.070690.
24. **Wilck N, Matus MG, Kearney SM, Olesen SW, Forslund K, Bartolomaeus H, Haase S, Mähler A, Balogh A, Markó L, Vvedenskaya O, Kleiner FH, Tsvetkov D, Klug L, Costea PI, Sunagawa S, Maier L, Rakova N, Schatz V, Neubert P, Frätzer C, Krannich A, Gollasch M, Grohme DA, Côrte-Real BF, Gerlach RG, Basic M, Typas A, Wu C, Titze JM, Jantsch J, Boschmann M, Dechend R, Kleinewietfeld M, Kempa S, Bork P, Linker RA, Alm EJ, Müller DN.** Salt-responsive gut commensal modulates T_H17 axis and disease. *Nature* 551: 585–589, 2017. doi:10.1038/nature24628.
25. **Wu CY, Zha H, Xia QQ, Yuan Y, Liang XY, Li JH, Guo ZY, Li JJ.** Expression of angiotensin II and its receptors in activated microglia in experimentally induced cerebral ischemia in the adult rats. *Mol Cell Biochem* 382: 47–58, 2013. doi:10.1007/s11010-013-1717-4.
26. **Xanthos DN, Sandkühler J.** Neurogenic neuroinflammation: inflammatory CNS reactions in response to neuronal activity. *Nat Rev Neurosci* 15: 43–53, 2014. doi:10.1038/nrn3617.
27. **Xiao L, Kirabo A, Wu J, Saleh MA, Zhu L, Wang F, Takahashi T, Loperena R, Foss JD, Mernaugh RL, Chen W, Roberts J II, Osborn JW, Itani HA, Harrison DG.** Renal Denervation Prevents Immune Cell Activation and Renal Inflammation in Angiotensin II-Induced Hypertension. *Circ Res* 117: 547–557, 2015. doi:10.1161/CIRCRESAHA.115.306010.
28. **Xie L, Choudhury GR, Winters A, Yang SH, Jin K.** Cerebral regulatory T cells restrain microglia/macrophage-mediated inflammatory responses via IL-10. *Eur J Immunol* 45: 180–191, 2015. doi:10.1002/eji.201444823.
29. **Xie L, Yang SH.** Interaction of astrocytes and T cells in physiological and pathological conditions. *Brain Res* 1623: 63–73, 2015. doi:10.1016/j.brainres.2015.03.026.
30. **Yang T, Ahmari N, Schmidt JT, Redler T, Arocha R, Pacholec K, Magee KL, Malphurs W, Owen JL, Krane GA, Li E, Wang GP, Vickroy TW, Raizada MK, Martyniuk CJ, Zubcevic J.** Shifts in the gut microbiota composition due to depleted bone marrow beta adrenergic signaling are associated with suppressed inflammatory transcriptional networks in the mouse colon. *Front Physiol* 8: 220, 2017. doi:10.3389/fphys.2017.00220.
31. **Yang T, Santisteban MM, Rodriguez V, Li E, Ahmari N, Carvajal JM, Zadeh M, Gong M, Qi Y, Zubcevic J, Sahay B, Pepine CJ, Raizada MK, Mohamadzadeh M.** Gut dysbiosis is linked to hypertension. *Hypertension* 65: 1331–1340, 2015. doi:10.1161/HYPERTENSIONAHA.115.05315.
32. **Zhang M, Malik AB, Rehman J.** Endothelial progenitor cells and vascular repair. *Curr Opin Hematol* 21: 224–228, 2014. doi:10.1097/MOH.0000000000000041.
33. **Ziv Y, Ron N, Butovsky O, Landa G, Sudai E, Greenberg N, Cohen H, Kipnis J, Schwartz M.** Immune cells contribute to the maintenance of neurogenesis and spatial learning abilities in adulthood. *Nat Neurosci* 9: 268–275, 2006. doi:10.1038/nn1629.
34. **Zoccal DB, Paton JF, Machado BH.** Do changes in the coupling between respiratory and sympathetic activities contribute to neurogenic hypertension? *Clin Exp Pharmacol Physiol* 36: 1188–1196, 2009. doi:10.1111/j.1440-1681.2009.05202.x.
35. **Zubcevic J, Jun JY, Kim S, Perez PD, Afzal A, Shan Z, Li W, Santisteban MM, Yuan W, Febo M, Mocco J, Feng Y, Scott E, Baekey DM, Raizada MK.** Altered inflammatory response is associated with an impaired autonomic input to the bone marrow in the spontaneously hypertensive rat. *Hypertension* 63: 542–550, 2014. doi:10.1161/HYPERTENSIONAHA.113.02722.
36. **Zubcevic J, Potts JT.** Role of GABAergic neurones in the nucleus tractus solitarii in modulation of cardiovascular activity. *Exp Physiol* 95: 909–918, 2010. doi:10.1113/expphysiol.2010.054007.
37. **Zubcevic J, Santisteban MM, Perez PD, Arocha R, Hiller H, Malphurs WL, Colon-Perez LM, Sharma RK, de Kloet A, Krause EG, Febo M, Raizada MK.** A single angiotensin II hypertensive stimulus is associated with prolonged neuronal and immune system activation in Wistar-Kyoto rats. *Front Physiol* 8: 592, 2017. doi:10.3389/fphys.2017.00592.
38. **Zubcevic J, Santisteban MM, Pitts T, Baekey DM, Perez PD, Bolser DC, Febo M, Raizada MK.** Functional neural-bone marrow pathways: implications in hypertension and cardiovascular disease. *Hypertension* 63: e129–e139, 2014. doi:10.1161/HYPERTENSIONAHA.114.02440.